Thermal Modelling of a Fractional-Slot Concentrated-Winding Kaman Type Axial-Flux Permanent-Magnet Machine

Gy. Vainel* and D. A. Staton

Motor Design Ltd.
Ellesmere
Shropshire, UK
dave.staton@motor-design.com

F. Giulii Capponi, G. De Donato and F. Caricchi

Dept. of Astronautical, Electrical and Energetic Engineering
University of Rome "La Sapienza"
Rome, Italy
fabio.giuliicapponi@uniroma1.it

Abstract— The aim of the paper is to present the thermal modeling of a Kaman type Axial-Flux Permanent-Magnet machine with fractional-slot concentrated-winding. This machine is air-cooled and equipped with specific arrangements to enhance heat dissipation. Thermal paths inside the machine are quite complex and require three-dimensional modelling. This is achieved through a lumped parameter network and subdivision of machine into cuboidal elements. The paper describes how thermal modeling is achieved and compares simulations with experimental results taken from a full scale prototype equipped with a number of thermocouples.

I. INTRODUCTION

Fractional-slot concentrated-winding (FSCW) axial-flux permanent-magnet (AFPM) machines have been the subject of a considerable amount of research due to their interesting properties and possible applications, from renewable energy systems to transportation, wherever extreme axial compactness coupled with high torque density and high efficiency are necessary, [1]. It has been demonstrated that the choice of a fractional number of slots per pole per phase increases leakage inductance, thus enhancing the flux-weakening capability, reduces cogging torque and can also allow for fault tolerance. Unfortunately, in FSCW machines rotor losses increase due to harmonic and sub-harmonic mmf waves. These loss components are critical because they are much more difficult to extract than those in the stator and can contribute significantly to excessive rotor temperature and consequent permanent magnet (PM) demagnetization. This disadvantage has prompted researchers to look for ways to reduce the impact of these losses. Furthermore, the diffusion of commercial software packages which simulate lumped thermal equivalent circuit models or computational fluid dynamics (CFD) has given researchers a powerful set of tools to perform complex simulations of heat generation, flow and exchange in AFPM machines, [2]-[5].

MMF induced losses are always present with FSCW, irrespective of the AFPM topology; however, the amount of losses depends on the resistivity of the PMs and of the rotor. Torus and single-stator single-rotor machines require rotors with back iron, while Kaman machines do not. In the latter, it is therefore possible to use high resistivity PM supports in order to reduce rotor losses. In [6], the design and finite element analysis validation of a 10 kW, 24 slot 20 pole Kaman type FSCW AFPM machine with tooth-wound coils was presented (Fig. 1). Three different variants of rotor disc were proposed, with the aim of minimizing the induced losses therein. This contribution is a continuation of the above paper, reporting the thermal modelling of the machine, carried out with a lumped thermal equivalent circuit model. After a brief recap of the electromagnetic design of the machine, the thermal model is described and simulation of the transient thermal performance of the machine is performed and compared to experimental tests on a full scale prototype.
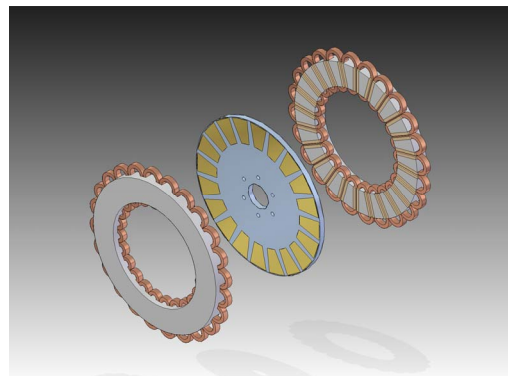

Figure 1. Exploded view of the Kaman type FSCW AFPM machine

II. THERMAL MODELLING METHODOLOGIES

Thermal analysis can be divided into two basic types: analytical lumped circuit and numerical methods. The analytical approach has the advantage of being very fast to calculate, but the developer of the network model must invest effort in defining a circuit that accurately models the main heat transfer paths [7-10]. Lumped circuit techniques are essential if the designer is to thermally evaluate many complex and long duty cycles.

In lumped circuit analysis, nodes are placed at important points on the motor cross-section, such as the stator back iron, tooth, winding hotspot, etc. These are linked by conduction, convection and radiation thermal resistances. Losses are input at the relevant nodes. Thermal capacitances are added to carry out thermal transient analysis. Flow

---

network analysis is used to calculate pressure drops and predict flow rates.

The basic formulations thermal resistances are quite simple. A conduction resistance is equal to the path length divided by the product of the path area and the materials thermal conductivity. Convection and radiation resistances are equal to one divided by the product of the surface area and the heat transfer coefficient. The radiation heat transfer coefficient is simply a function of the surface properties i.e. the emissivity and the view factor. The emissivity is known for different types of surface and the view factor can be calculated based on the geometry. The convection heat transfer coefficient is most often based on empirical formulations based on convection correlations which are readily available in the heat transfer literature [11-16]. Fortunately, there are a wealth of convection correlations for most of the basic geometric shapes used in electrical machines, both for natural and forced convection cooling i.e. cylindrical surfaces, flat plates, open fin channels, closed fin channels, etc.

A more accurate estimation of the 3-dimensional nature of conduction heat transfer can be gained by the use of special cylindrical and cuboidal thermal resistance components [7, 17]. These components mathematically distribute the losses evenly throughout the volume and allow for an anisotropic thermal conductivity.

The main strength of numerical analysis is that any device geometry can be modelled. However, it is very demanding in terms of model setup and computational time. There are two types of numerical analysis: Finite Element Analysis (FEA) and Computational Fluid Dynamics (CFD). CFD has the advantage that it can be used to predict flow in complex regions such as around the motor end windings [18, 19]. FEA can only be used to model conduction heat transfer in solid components. For convection boundaries, the same analytical/empirical algorithms used in the lumped circuit analysis must be adopted i.e. convection correlations. Best use of time demanding numerical analysis is to help develop improved analytical algorithms and calibrate lumped circuit models.

III. ELECTROMAGNETIC DESIGN

Rated values of the Kaman type FSCW AFPM machine chosen for the study are reported in Tab. I, while Tab. II shows its main geometrical dimensions. A complete description of the electromagnetic design has already been given in [6] and, therefore, only main characterizing aspects are here recalled.

Among the particular manufacturing solutions chosen in this design, flat ribbon conductors have been used for the stator concentrated coils , thus achieving a high slot fill factor, i.e. > 0.7. The specific case of flat ribbon conductors brings about a manufacturing complication, since the conductors must be bent in the direction which offers the highest mechanical stiffness. This requires a considerable bending moment to be applied to the conductor and the resulting radius of curvature is much larger than that of the core-wound coil. A double layer winding (all teeth wound) has been chosen since it requires shorter end connections. SMC wedges with non-magnetic gaps are used to close the

slots and therefore to reduce the loss-inducing permeance harmonics.

TABLE I: RATED VALUES OF THE KAMAN FSCW AFPM PROTOTYPE (ASSUMING FORCED VENTILATION)

Rated power	10 kW
Rated torque	120 Nm
Rated speed	800 rpm
Rated phase back-emf	85 V
Rated current	40 A
Rated frequency	133.3 Hz

TABLE II: GEOMETRIC PARAMETERS OF THE KAMAN FSCW AFPM PROTOTYPE

Number of pole pairs	10
Number of slots	24
Outer active radius	148 mm
Inner active radius	100 mm
End connection outer radius	167 mm
Stator yoke thickness	11 mm
Slot width	14 mm
Slot height	14 mm
Conductor size	6.3x1 mm (6.085 mm^2)
Turns per coil	18 (2x9)
Series turns per phase	144
Slot fill factor	0.78
SMC wedge thickness	2.5 mm
Wedge gap width	3 mm
Magnet average width	29 mm
Total magnet thickness	2 x 5 mm
Total mechanical air-gap	2 x 2 mm
Total axial length	64 mm

In Kaman type AFPM machines, the rotor disc has a purely structural purpose, i.e. it supports the PMs. In order to limit induced losses, the disc is made of stainless steel and its design has been optimized by segmenting the external retaining ring. In this way, the induced eddy losses are kept at bay since the circulation paths of the sub-harmonic MMF induced eddy currents are interrupted. Fig. 1 shows an exploded view of the prototype, without the frame and the cooling system.

While a number of specific arrangements have been included in order to reduce losses, still providing adequate cooling paths is critical, specifically because of the additional losses induced by the FSCW winding type.

The Kaman topology is inherently suited for air cooling. This is due to the fact that the stator backs are rigidly connected to end shields; if a thermally conductive material such as aluminium is used and if the shields are equipped with fins on their exterior, it is possible to use them as heat sinks, through which the heat generated in the stators is dissipated by forced ventilation.

Moreover, the connection between stator back iron and the housing can be filled up with high thermal conductivity heat paste, thus making a good conduction path from coils to housing through the stator.

Finally, it is also possible to pot the outer endwindings connections. In this case, a direct conduction path from coil to the housing is created, allowing the machine to operate at higher power levels or have longer expected lifetime at same power level.

A lumped circuit model that can predict the transient thermal performance of the axial flux motor topology described above has been created in the PORTUNUS, [20], system simulation software package. The model is fully parameterized. EXCEL is used as a pre- and post-processing user interface. The EXCEL interface is scripted to calculate the parameters needed for the system simulation model and automatically load this data into the simulation. The main output temperature predictions from model are ported back into EXCEL, where they are displayed in tabular and graphical forms. Detailed simulation results are saved into new updated PORTUNUS model file. The loss data is imported from the electromagnetic design.

Symmetry along the axial length means that it is possible to model just half the machine, one stator and half the rotor as shown in Fig 2. The same figure also shows the main dissipation paths in the machine. Red arrows are for conduction and blue arrows for convection paths. If the outer end windings are potted into the housing and end-caps to aid cooling of the coils, then the heat transfer changes from convection to conduction in that region.

Also, circumferential symmetry has been applied to simplify modelling of the machine

The analysis in this paper is concentrated on prediction of the internal conduction heat transfer and convection heat transfer across the airgap. External convection heat transfer will be the subject of a follow on project. In this analysis, it is assumed to have a certain level of external cooling, which results in fixed housing temperature.
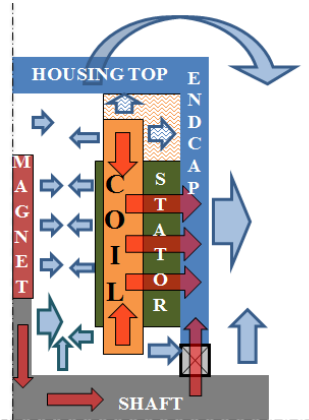

Figure 2. Cross section of half machine, showing thermal paths
(red arrows for conduction, blue arrows for convection)

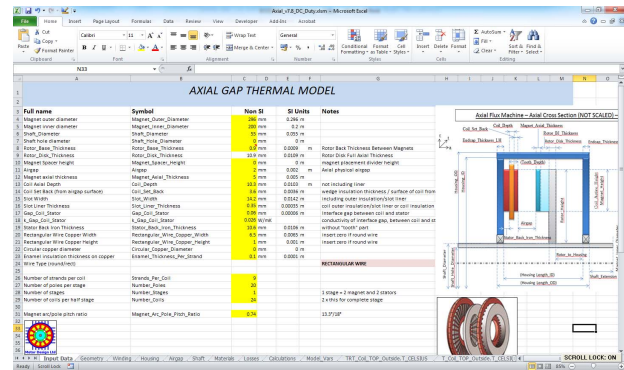### A. EXCEL Interface to Thermal Model

The EXCEL interface is spread over several worksheets. This allows the input data to be split into logical sections such as Input Data, Geometry, Winding, Airgap, Shaft, Materials, Losses, Calculations and Model Variables. The Input Data worksheet is shown in Fig. 3. This screen capture is for illustration purposes only, i.e. the cell names are too small to read but it is only provided in the paper to give an indication of the type of information presented in the worksheets. Input data is highlighted in yellow. Diagrams are supplied on the worksheets to help the designer interpret

the data required as input and the calculated data presented. EXCEL equations are used to calculate the details of geometry, the component weights from motor dimensions (used in thermal capacitance calculation), airgap heat transfer (convection correlations), loss components and equivalent slot thermal conductivity.

Airgap convection heat transfer is calculated using rotational Reynolds number based correlations as given in [4]. This method indicates typical convection heat transfer values in the ranges 20 W/m^{2}K to 70 W/m^{2}K for the motor under consideration. Aigap convection aids in cooling of the magnets, the other main cooing path being through conduction to the shaft.

Loss definition requires only phase resistance (at ambient temperature), applied phase RMS current (with or without duty cycle) and total losses. Losses are then split into copper losses, iron losses and magnet losses and applied to the relevant nodes using pre-calculated ratios. The ratios can be obtained from electromagnetic design, FEA or experimental tests. In this case, experimental results were available [6], so that total losses were measured. Separation of iron losses (including the ones generated by MMF harmonics) and rotor losses was done with the help of FEA, but it was also verified experimentally through differential tests. Excluding copper losses, the remaining losses were divided as follows: 53.6% are spread over the stator tooth, 35.7% over the back iron, 7.1% over the magnet and 3.6% over the rotor disc.

The equivalent slot thermal conductivity of the double layered flat ribbon coils was calculated in EXCEL with three simple thermal resistances in series representing the pure copper, the enamel insulation layer on top of the copper and the impregnation in the slot. In turn, each thermal resistance is calculated through the geometry and the masses inside the slot.

Figure 3. Excel interface for PORTUNUS lumped parameter model

B. Lumped Circuit Thermal Model

The particular system simulation software used [20] has a robust non-linear transient solver that is used to solve the thermal lumped circuit and makes use of a drag and drop user interface to prototype the circuit. It also supports VHDL-AMS library component model development. This was used to create a number of new library components such as the cuboidal element that allows accurate prediction of 3-dimensional conduction heat transfer [17].

As indicated in Fig. 2, the thermal paths inside the machine are quite complex and require a three-dimensional

heat transfer model. In order to manage this complexity, the complete thermal network is divided into worksheets, each of them representing a slice of the machine along the axial direction. Five slices exist, as shown in Fig. 4, modelling the rotor, airgap, coils, stator back iron and endcaps. Slices are then connected together, as needed, in order to add the third dimension.

To help understanding the general complexity of the thermal circuit developed, the coil and tooth slice is represented in more detail in Figs. 5 and 6. In particular, Fig. 5 shows a portion of the stator, detailing two coils and teeth. Superimposed in the same pictures are drawn the cuboidal elements related to the coil and tooth slice. The same cuboidal elements are then visible in Fig. 6 on the corresponding Portunus worksheet. It is possible to recognize that three cuboids are used to model each of the two coil sides, while one cuboid is used for each of the coil end windings. Three further cuboids are used inside the coil for the central iron tooth.

Sheet ports are used to connect the thermal circuit across worksheets (i.e. slices), to the airgap at one side and to the back iron on the other side in the case of Fig. 6. In this way it is possible to accurately model three-dimensional heat paths.

Loss scaling is used in the model to account for the copper loss variation with winding resistance which itself is a function of temperature. Current design uses typical 0.00393 1/K copper (linear) thermal coefficient. Loss scaling is also used to vary the iron and magnet loss with speed.
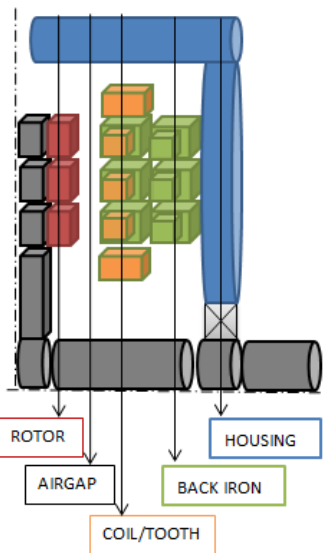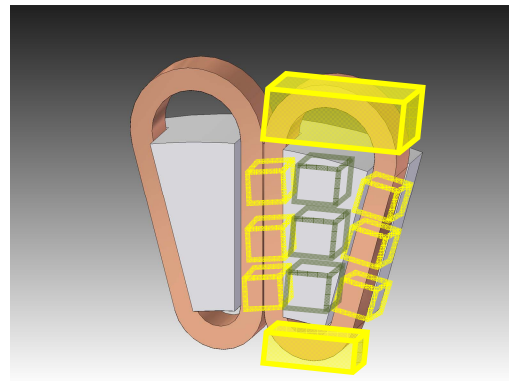

Figure 5. Drawing of coil and tooth cross section with superimposed cuboidal elements
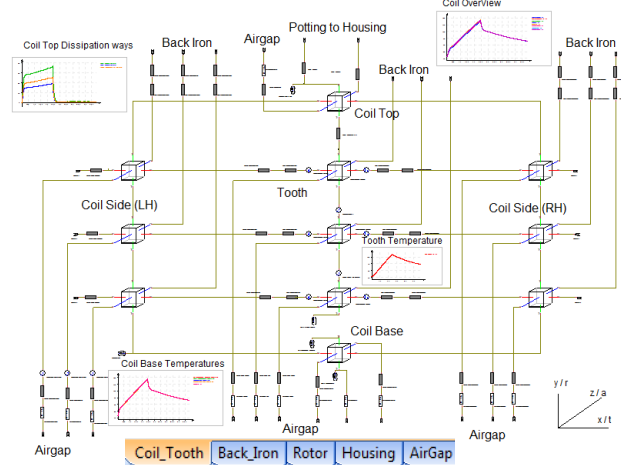

Figure 6. Coil and tooth slice corresponding to Fig. 5, as a worksheet in in Portunus environment

V. EXPERIMENTAL VALIDATION

A range of experimental tests have been made to validate the model. The machine has been mounted on a test bench equipped with a Hottinger Baldwin Messtechnik T10 torque flange and a Yokogawa PZ4000 Power Analyzer.

Several thermocouples were put within the motor cross-section and motor temperatures were recorded at each time step, together with losses. In total, 2x10 pc of K-type thermocouples were built into the machine: first 10 pc for one half of the machine and the other 10pc for the other half of the machine. Table III sums up the location of the applied thermocouples, while Fig. 7 shows their placement inside the machine.

Figure 4. Schematic representation of the machine, showing the main cuboidal elements and their belonging to different slices

TABLE III: LOCATION OF THE THERMOCOUPLES

| No.	Name	Position
1,2	End Winding Top coil	Center of outer end winding
3,4	End winding Bottom coil	Centre of inner end winding
5,6	Entrance of slot	Between two coils at the entrance of slot
7	Stator back Iron	Inside the stator back iron, in the middle of the yoke
8	Stator back Iron top	On the upper face of yoke
9	Housing outer	On the side of housing near fins
10	Housing inner	On housing, near bearing
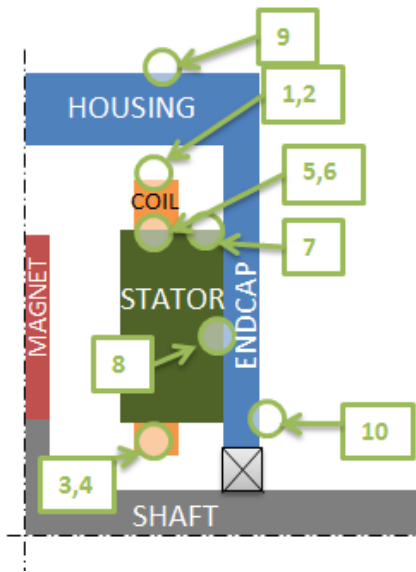
Figure 7. Sketch of thermocouples placement inside the machine

A first set of tests was performed by feeding a range of DC current values into the winding, so that the resultant thermal model is greatly simplified having a single loss source. DC tests have been conducted with both natural and forced convection cooling.

The aim of the tests was to calibrate the thermal model to account for manufacturing based uncertainties such as the goodness of the fit between components. It is impossible to have perfect contact between surfaces of different materials, for example, between the back iron and the housing. These are often modeled as equivalent airgaps (named "interface gaps"). The gaps cannot be physically measured, but the DC test allows them to be determined experimentally.

Figure 8 shows the typical goodness of the fit between test and calculated transient temperatures after model tuning. In particular, Fig. 8a represents the plot for the copper temperature at the slot entrance, while Fig. 8b shows the same plot for the temperature inside the stator back-iron. Blue curves represent tests results and red curves predictions from simulation.

Furthermore, for this machine it was possible to perform the tests both for non-potted and for potted endwindings. Figure 9 shows the same temperature plots of Fig. 8, but for the case of machine with potted endwindings.

Potting transforms the endwindings-to-housing heat path from convection to conduction. An evaluation of the effectiveness of this change can be gained by calculating the ratio of endwinding-to-housing temperature difference for the two cases, both having the same current values. In this case, it is estimated that potting provided a reduction in equivalent endwinding-to-housing thermal resistance of approximately 25%.

Finally, having fixed the interface gaps, a full range of AC tests (up to 1.5 p.u. current) were performed with the machine running. Tests were performed with the machine at 1 p.u. and at 2 p.u. speed. This second speed was selected in order to enhance the effect of MMF induced rotor losses and evaluate the fitness of the calculated airgap convection heat transfer.

Figures 10 and 11 show an example of the obtained results, for the case of AC tests at 30A current, in which the machine reaches a steady state even with natural cooling. Figure 10 represents temperature predictions from the model, while Fig. 11 shows the equivalent recorded values from experimental test. For each test, in order to better evaluate how the model fits with experiments, final temperature values were directly compared, as in Table IV.

From the analysis of the whole set of results, a few considerations can be drawn. In steady state conditions errors are, typically, in the range 2-3 % and reach a maximum of 6%. Values of this kind are within the measurement error range and therefore should be considered a very good fit. The model is also capable of a predicting the thermal transients with good accuracy, i.e. with a maximum error of below 10%. This was somehow expected, since we can easily predict component weights and so make an accurate prediction of the thermal capacitances.

From the analysis of Figs. 10 and 11 it is also possible to understand the effectiveness of applying high thermal conductive heat paste between the stator back iron and housing. In fact the temperature build up at this important interface, which is directly in the main dissipation path for cooling, is almost negligible.

I. CONCLUSIONS

In this paper, a thermal model for a Kaman type FSCW AFPM machine with tooth-wound coils has been presented. The model is based on a lumped parameter network, capable of reproducing three-dimensional thermal paths. The network is composed by cuboidal elements which allow a more accurate estimation of the 3-dimensional nature of conduction heat transfer.

The model structure allows visualization of the complex thermal paths inside the machine and therefore helps designers understand in which areas they need to concentrate effort to meet the requirements of their applications and to study the effect of changing different parameter sets.

An accurate thermal model can be obtained using an equivalent slot thermal conductivity based on a pre-defined analytical algorithm that is a function of the amount of different materials in the slot. Estimates of the effective interface gaps can also be based on previous experience, but improved accuracy can be obtained by calibration using a simplified DC current test.

The same thermal model gives a good match for a wide range of operational points, including overload. The model is able to capture both steady state and transient behavior with very good accuracy. It is possible to use the model to perform complex duty cycle analysis and evaluate the machine's expected lifetime.

Results have also demonstrated the effectiveness of two arrangements that have been included in this machine in order to enhance heat exchange. Adoption of endwinding potting significantly increases machine's capability to operate at high duty cycles with a cooler winding hot spot. This is due to a combination of the additional winding thermal capacitance and the direct thermal conductive heat path from endwindings to housing.

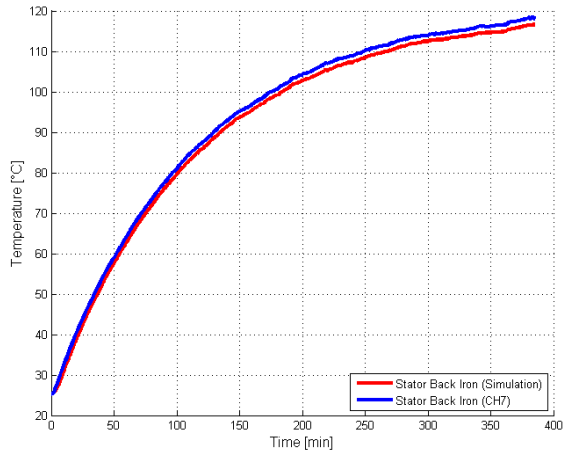Also, applying high thermal conductive heat paste between the stator back iron and housing gives an almost negligible temperature build up at this important interface, which is directly in the main dissipation path for cooling.
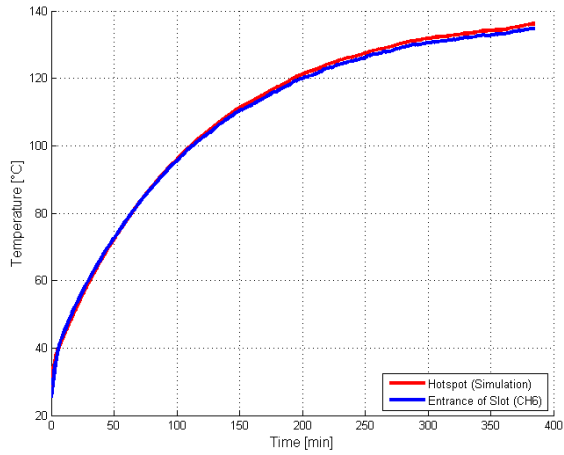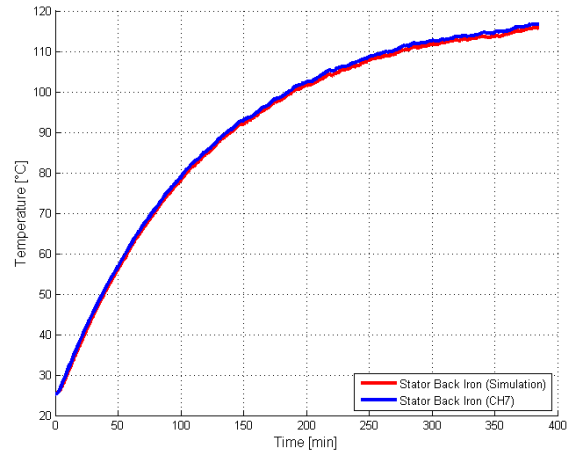

a) Copper temperture at coil entrance
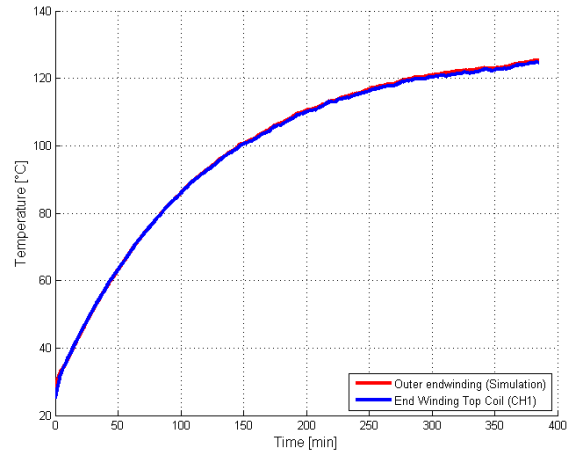
b) Stator back iron temperature

Figure 8. 30 A DC tests. Non-potted endwindings, natural convection

a) Copper temperture at coil entrance

b) Stator back iron temperature

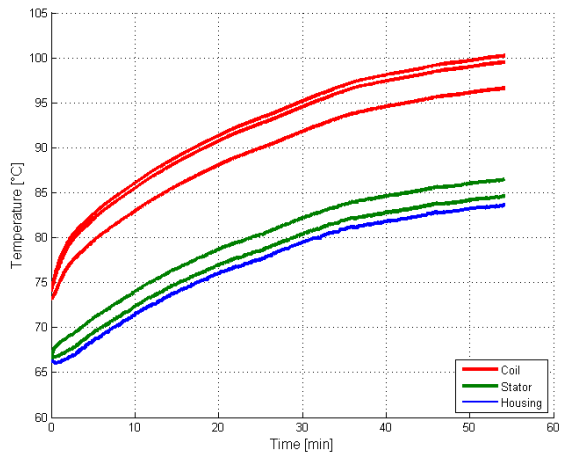Figure 9. 30 A DC tests. Potted endwindings, natural convection

Figure 10. 30A AC simulation temperature prediction

Figure 11. 30A AC test results
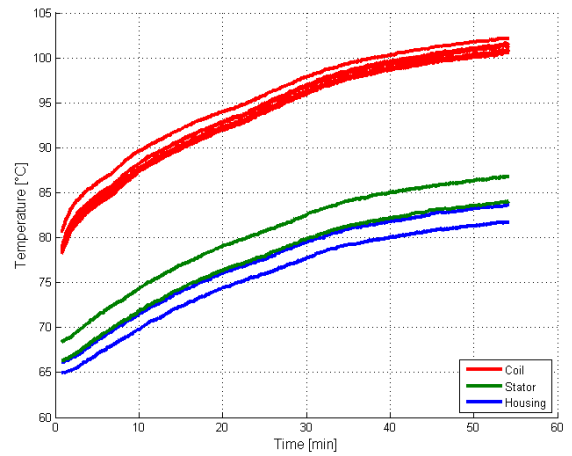
TABLE IV: FINAL VALUES OF 30A AC TEST AND SIMULATION

No	Location	Test		Simulation	
1	End Winding Top coil	100.7	°C	96.6	°C
2	End Winding Top coil	101.3	°C	96.6	°C
3	End winding Bottom coil	100.5	°C	100.2	°C
4	End winding Bottom coil	100.7	°C	100.2	°C
5	Entrance of slot	101.6	°C	99.5	°C
6	Entrance of slot	102.1	°C	99.5	°C
7	Stator back Iron	86.8	°C	84.6	°C
8	Stator back Iron top	84.0	°C	86.5	°C
9	Housing outer	83.6	°C	83.6	°C
10	Housing inner	81.7	°C	83.6	°C

REFERENCES

[1]   F. Giulii Capponi, G. De Donato and F. Caricchi, "Recent advances in axial-flux permanent-magnet machine technology", *IEEE Trans. Ind. Appl.*, vol. 48, no. 6, pp. 2190–2205, Nov./Dec. 2012.

[2]   F. Marignetti, V. Delli Colli and Y. Coia, "Design of axial flux PM synchronous machines through 3-D coupled electromagnetic thermal and fluid-dynamical finite-element analysis" *IEEE Trans. on Ind. Electron.*, vol. 55, no. 10, pp 3591-3601, Oct. 2008.

[3]   C.H. Lim, J.R. Bumby, R.G. Dominy, G.I. Ingram, K. Mahkamov, N.L. Brown, A. Mebraki and M. Shanel, "2-D lumped-parameter thermal modelling of axial flux permanent magnet generators" in proc. *ICEM*, pp 1-6, Sep. 2008.

[4]   D.A. Howey, A.S. Holmes and K.R. Pullen, "Measurement and CFD prediction of heat transfer in air-cooled disc-type electrical machines" *IEEE Trans. Ind. Appl.*, vol. 47, no. 4, pp 1716-1723, Jul./Aug. 2011.

[5]   Y.C. Chong, J. Chick, M.A. Mueller, D.A. Staton and A.S. McDonald, "Thermal modelling of a low speed air-cooled axial flux permanent magnet generator" in proc. *IET PEMD*, pp. 1-7, Mar. 2012.

[6]   F. Giulii Capponi, G. De Donato, G.A. Rivellini and F. Caricchi, "Fractional-slot concentrated-winding axial-flux permanent-magnet machine with tooth-wound coils", in Proc. *ICEM*, pp. 281-287, Sep. 2012.

[7]   P.Mellor, D.Roberts, D. Turner, "Lumped parameter thermal model for electrical machines of TEFC design", IEE Proceedings, Vol. 138, September 1991, pp. 205,218.

[8]   A.Boglietti, A. Cavagnino, M. Lazzari, M. Pastorelli "A simplified thermal model for variable speed self cooled industrial induction motor", IEEE Transaction on Industry Application, Vol.39, n.4 July August 2003, pp.945-952.

[9]   G. Kylander, "Temperature Simulation of a 15kW Induction Machine Operated at Variable Speed", ICEM92, Manchester, 15-17 Sept., 1992.

[10]   D.A. Staton, "Thermal Computer Aided Design" - Advancing the Revolution in Compact Motors, IEEE IEMDC 2001, Boston, USA, June 2001.

[11]   J.P. Holman, Heat Transfer, McGraw-Hill, 1997, ISBN 0-07-844785-2.

[12]   A.F. Mills, Heat Transfer, Prentice Hall, 1999, ISBN 0-13-947624-5.

[13]   J.R. Simonson, "Engineering Heat Transfer" 2nd Edition, McMillan, 1998, ISBN 0-333-45999-7.

[14]   A. Bejan, Heat Transfer, Wiley, 1993, ISBN 0-471-50290-1

[15]   W.S. Janna, Engineering Heat Transfer, Van Nostrand Reinhold (International), 1988, ISBN 0-278-00051-7.

[16]   F.P. Incropera, D.P. De Witt, Introduction to Heat Transfer, Wiley, 1990, ISBN 0-471-51728-3.

[17]   R. Wrobel, P.H. Mellor, "A General Cuboidal Element for Three-Dimensional Thermal Modelling",   IEEE Transactions on Magnetics, Vol 46 , no.8. pp., 3197-3120, Aug. 2010.

[18]   J. Mugglestone, S.J. Pickering, D. Lampard, "Effect of Geometry Changes on the Flow and Heat Transfer in the End Region of a TEFC Induction Motor", 9th IEE Intl. Conf. Electrical Machines & Drives, Canterbury, UK, Sept 1999.

[19]   D.A. Staton, S.J. Pickering, D. Lampard, "Recent Advancement in the Thermal Design of Electric Motors", SMMA 2001 Fall Technical Con., Durham. North Carolina, 3-5 Oct. 2001.

[20]   http://www.adapted-solutions.com/web/AdaptedSolutionsEnglish/ASProductPortunus.html